TAM Family Receptor kinase inhibition reverses MDSC-mediated suppression and augments anti-PD-1 therapy in melanoma.

Alisha Holtzhausen[1], **William Harris**[1], **Eric Ubil**[1], **Debra M. Hunter**[1], **Jichen Zhao**[2], **Yuewei Zhang**[2], **Dehui Zhang**[2], **Qingyang Liu**[2], **Xiaodong Wang**[2], **Douglas K. Graham**[3], **Stephen V. Frye**[1,2], **H. Shelton Earp**[1,4,*]

[1.]UNC Lineberger Comprehensive Cancer Center, Department of Medicine, School of Medicine, University of North Carolina at Chapel Hill, Chapel Hill, NC

[2.]Center for Integrative Chemical Biology and Drug Discovery, Division for Chemical Biology and Medicinal Chemistry, Eshelman School of Pharmacy, University of North Carolina at Chapel Hill, Chapel Hill, NC

[3.]Aflac Cancer and Blood Disorders Center of Children's Healthcare of Atlanta, Department of Pediatrics, School of Medicine, Emory University, Atlanta, GA

[4.]Department of Medicine, Pharmacology, University of North Carolina at Chapel Hill, Chapel Hill, NC

Abstract

Myeloid cell receptor tyrosine kinases (RTK) TYRO3, AXL and MERTK and their ligands, Gas 6 and Protein S, physiologically suppress innate immune responses, including in the tumor microenvironment. Here, we showed that myeloid-derived suppressor cells (MDSCs) dramatically upregulated TYRO3, AXL and MERTK and their ligands (M-MDSCs>20-fold, PMN-MDSCs>15-fold) in tumor-bearing mice. MDSCs from tumor bearing $Mertk^{-/-}$, $Axl^{-/-}$ and $Tyro3^{-/-}$ mice exhibited diminished suppressive enzymatic capabilities, displayed deficits in T cell suppression and migrated poorly to tumor-draining lymph nodes (TDLNs). In co-implantation experiments, using TYRO3$^{-/-}$, AXL$^{-/-}$ and MERTK$^{-/-}$ MDSCs, we showed the absence of these RTKs reversed the pro-tumorigenic properties of MDSCs *in vivo*. Consistent with these findings, *in vivo* pharmacologic TYRO3, AXL and MERTK inhibition diminished MDSCs' suppressive capability, slowed tumor growth, increased CD8$^+$ T cell infiltration and augmented anti-PD-1 checkpoint inhibitor immunotherapy. Mechanistically, MERTK regulated MDSC suppression and differentiation in part through regulation of STAT3 serine phosphorylation and nuclear localization. Analysis of metastatic melanoma patients demonstrated an enrichment of circulating MERTK$^+$ and TYRO3$^+$ M-MDSCs, PMN-MDSCs and e-MDSCs relative to these MDSC populations in healthy controls. These studies demonstrated that TYRO3, AXL and MERTK

*Correspondence to: Shelton_Earp@med.unc.edu, H. Shelton Earp III, M.D., Professor and Director, UNC Lineberger Comprehensive Cancer Center, Professor of Medicine and Pharmacology, The School of Medicine, The University of North Carolina at Chapel Hill, 450 West Drive CB 7295, Chapel Hill, NC 27599-7295, Telephone: 919.966.2335, Fax: 919.966.3015.

control MDSC functionality and serve as promising pharmacologic targets for regulating MDSC-mediated immune suppression in cancer patients.

Introduction.

A high number of tumor-infiltrating lymphocytes (TILs) is associated with a better prognosis for advanced melanoma, breast and lung cancer (1–3). This and emerging data suggest targeting the host immune system can enhance cancer therapies(4). While some patients have a positive response to immunotherapy, the majority remain refractory (5). A better understanding of the entire immunosuppressive landscape - both the adaptive and the innate systems - is necessary to improve this promising treatment modality.

The overall melanoma response rate of the CTLA-4 antagonist, ipilimumab, is ~10% and the PD-1 antagonist, pembrolizumab, exceeds 35% (6,7). A lack of functional or tumor-infiltrating T cells are often cited as reasons for therapeutic failure (8,9). Several additional T cell-centric therapies are currently being investigated in clinical trials (10–14). While many acknowledge the importance of the myeloid compartment in the tumor microenvironment (TME), including tumor-associated macrophages (15,16) MDSCs (17,18) and tolerizing or inactive antigen presenting cells (APCs) (19,20), cancer therapeutics based on the innate immune system are less common (e.g. IDO and PI3K-γ inhibitors (21–23)). To increase the efficacy and durability of immunotherapy, additional methods reversing the immunosuppressive TME and a better understanding of immunotherapy resistance mechanisms are needed.

TYRO3, AXL, MERTK transmembrane receptor tyrosine kinases (TAM RTKs) regulate the innate immune system, dampening inflammatory responses to prevent chronic inflammation and auto-immunity (24,25). The activity of these receptors is stimulated by protein ligands e.g. GAS6 and PROTEIN S (26,27). The protein ligands have a higher affinity and are most effective when they bridge the cell surface TAM receptors to a source of lipid phosphatidylserine (PtdSer) exposed on apoptotic cells, aggregating platelets, exosomes and certain viruses that expose PtdSer on their surface (apoptotic mimicry) (24). GAS6 and PROTEIN S are expressed in multiple cell types including epithelial and immune cells (28) and can be secreted by tumor cells dampening the immune response (29). Genetic deletion of MERTK in mice leads to heightened inflammatory responses and mild auto-immunity (30). When tumors are implanted in $Mertk^{-/-}$ mice, tumor growth is slower and metastasis is decreased (31).

MDSCs are a heterogeneous population of bone marrow-derived, immature myeloid cells (17,32–34). MDSCs are potently immunosuppressive and have been implicated in negative regulation of immune responses during infection, cancer and the maternal immune response to fetuses (35–37). MDSCs promote tumor growth and metastasis by suppressing the anti-tumor immune response and through paracrine secretions that stimulate tumor cell proliferation, motility and angiogenesis (32). MDSCs correlate with poor prognosis in human melanoma and with lymph node metastasis in breast cancer patients (38,39). In mice, there are two MDSC subsets: monocytic (M-MDSC) and granulocytic or polymorphonuclear (PMN-MDSC). M-MDSCs are characterized by expression of CD11b

$^+$Ly6G$^-$Ly6C^{high} and PMN-MDSCs by CD11b$^+$Ly6G^{high}Ly6C^{low} (32). M- and PMN-MDSCs utilize diverse mechanisms to thwart T cell proliferation including increased activity of arginase 1 (Arg), indoleamine-2,3-dioxygenase (IDO), inducible nitric oxide synthase (iNOS), production of reactive oxygen species (ROS) as well as antigen-specific suppression (32). One factor controlling MDSC biology is the transcription factor STAT3 (signal transducer and activator of transcription 3), which regulates MDSC expansion and promotes MDSC survival (32). STAT3 also prevents differentiation of MDSCs to macrophages and DCs (40), in effect maintaining a more immunosuppressive microenvironment.

We investigated the contribution of TAM RTKs and ligands in MDSC function using *Mertk*$^{-/-}$, *Axl*$^{-/-}$ *and Tyro3*$^{-/-}$ mice and TYRO3, AXL and MERTK inhibitors. Genetic deletion or pharmacologic inhibition of TYRO3, AXL and MERTK diminished MDSC suppression in a STAT3 dependent manner. Additionally, inhibition of TYRO3, AXL and MERTK delayed the growth of a syngeneic melanoma model, enhanced T cell infiltration into the TME, and augmented the efficacy of anti-PD1 therapy. We showed that metastatic melanoma patients exhibit increased numbers of TYRO3$^+$, AXL$^+$ and MERTK $^+$ MDSCs, with MERTK$^+$ MDSCs predominating. These results suggest that TYRO3, AXL and MERTK cooperate as immunosuppressive, innate immune checkpoint genes across the myeloid spectrum with potential therapeutic import.

Materials and Methods.

In vivo Animal Studies:

C57BL/6J and OT-I (C57BL/6-Tg(TcraTcrb)1100Mjb/J) mice were purchased from Jackson Labs. *Mertk*$^{-/-}$, *Axl*$^{-/-}$ and *Tyro3*$^{-/-}$ mice are on a C57BL/6 background. *Mertk*$^{-/-}$ mice were derived by our lab and *Axl*$^{-/-}$ and *Tyro3*$^{-/-}$ mice were provided by Douglas K. Graham (Emory University, USA). Mice were genotyped by PCR to confirm gene deletion.

Tumor studies: 500,000 BRAF^{V600E}PTEN$^{-/-}$ cells were subcutaneously injected into syngeneic mice and allowed to form tumors. Tumors were measured by caliper every other day. Tumor volume was calculated according to the formula: cm^3 = [(length (cm) $\times$ (width (cm))^2]/2. 25mg/kg UNC4241 dissolved in saline or a saline vehicle was administered daily by oral gavage in a 100μl volume.

Gr-1 Depletion study: Tumor-bearing mice were injected with 200μg rat IgG2b isotype control or anti-mouse Ly6G/Ly6C (Gr-1) antibody (Clone RB6–8C5, BioXCell) every 3 days(36).

α-PD-1 treatment study: Tumor-bearing mice were injected with 250μg rat IgG2a isotype control or anti-PD-1 antibody (Clone RMP1–14, BioXCell) every 3 days (41).

Co-implantation study: FACS sorted MDSCs and BRAF^{V600E}PTEN$^{-/-}$ cells were mixed at a 1:10 MDSC:tumor cell ratio to mimic physiological conditions (42) and injected into syngeneic mice. Tumor volume was assessed as above.

All experimental groups included randomly chosen littermates, 8–10 weeks old of both sexes. Animal protocols (IACUC Protocol # 16–175) were approved by the Institutional Animal Care and Use Committee at UNC.

Cell Lines:

The BRAF^{V600E}PTEN$^{-/-}$ melanoma cell line was previously generated (43). Cell lines were cultured no longer than two weeks and were received in 2013 from the Hanks Lab (Duke University). Cells were not authenticated in the past year. Cells are cultured with a mycoplasma removal agent (MP Bio) to prevent contamination and were tested monthly with a PCR-based assay (Universal Mycoplasma Detection Kit, ATCC 30–1012K).

Flow Cytometry:

1,000,000 tumor, spleen or lymph node cells (obtained as described below) were stained with Live Dead stain (Thermo Fisher L34957) in PBS for 20 minutes. The reaction was quenched by adding RPMI with 5% FBS (fetal bovine serum) and centrifuging for 5 minutes at 1700 rpm at room temperature. Cell pellets were resuspended in flow buffer (PBS with 2% bovine serum albumin (BSA)) 1μg of each fluorochrome conjugated antibodies was added and incubated for 1 hour at room temperature in the dark. After staining 2ml of flow buffer was added and centrifuged for 5 minutes at 1700 rpm at room temperature. Samples were fixed with 2% paraformaldehyde in flow buffer for 15 minutes then washed with flow buffer. Samples were resuspended in flow buffer and analyzed using a LSRFortessa (Becton Dickinson) Data was analyzed using FlowJo software (Becton Dickinson) or FCS Express (Denovo Software).

MDSC Induction and Isolation:

Mice were subcutaneously injected with 500,000 BRAF^{V600E}PTEN$^{-/-}$ cells and allowed to form tumors. When tumors reached 1000mm^3 the mice were euthanized, and their spleens harvested. We enriched CD11b$^+$ cells using the EasySep Mouse CD11b Positive Selection Kit (Stemcell Technologies, 18970). Briefly, the selection cocktail was added to cells and incubated for 5 minutes before RapidSpheres were added and the mixture was incubated for 3 minutes. The sample tubes were inserted into the magnet ("The Big Easy" EasySep Magnet, Stemcell Technologies, 18001) for 5 minutes and the supernatant discarded. Remaining cells were washed with column buffer and subjected to magnetic isolation again. Isolated cells were then stained for Ly6C and Ly6G as described above and sorted on a FACSAria III (Becton Dickinson) instrument. See Supplemental Figure 1 for gating strategy.

Tumor Processing:

Tumors were harvested, minced with a razor blade and digested with RPMI containing collagenase IV (1 mg/ml), hyaluronidase (0.1mg/ml), and deoxyribonuclease (20 U/ml, Sigma) at 37°C for 1 hour then filtered through a 40μM filter for downstream applications.

RNA Isolation and qRT-PCR:

Total RNA was isolated using the RNeasy Plus Mini Kit (Qiagen, 74134) and quantified with a NanoDrop. 100ng RNA was reverse transcribed to cDNA using SuperScript IV VILO

Master Mix (ThermoFisher, 11756050). Real-time PCR was performed in triplicate using 5ng RNA on a ViiA 7 Real-Time PCR System (ThermoFisher). Taqman probes (*Tyro3* Mm00444547_m1), *Axl* (Mm00437221_m1), *Mertk* (Mm00434920_m1), *Gas6* (Mm00490378_m1), *Pros1* (Mm01343426_m1)) (ThermoFisher) or validated primers (below) and PowerUp SYBR Green Master Mix (ThermoFisher, A25742) were used for conventional qPCR. GAPDH was used as a reference gene for normalization and gene expression was determined using the $2^{-\Delta\Delta CT}$ method.

Primers: Arg Forward: 5' CTCCAAGCCAAAGTCCTTAGAG 3' Reverse: 5' AGGAGCTGTCATTAGGGACATC 3'

Nos2 Forward: 5' AGGAAGTGGGCCGAAGGAT 3' Reverse: 5' GAAACTATGGAGCACAGCCACAT 3'

Gapdh Forward: 5' GTCTACATGTTCCAGTATGACTCC 3' Reverse: 5' AGTGAGTTGTCATATTTCTCGTCGT 3'

Ido1 Forward: 5' CAGGCCAGAGCAGCATCTTC 3' Reverse: 5' GCCAGCCTCGTGTTTTATTCC 3'

Tgfb1 Forward: 5' CTCCCGTGGCTTCTAGTGC 3' Reverse: 5' GCCTTAGTTTGGACAGGATCTG 3'

ROS Production Assay:

10,000 MDSCs were plated in a black 96-well plate (Costar, 3916) and incubated overnight at 37°C with 5% CO_2. ROS Production was measured by DCFDA cellular ROS detection assay kit (Abcam, ab113851) according to manufacturer's directions. Fluorescence was measured at 535nm with an EnSpire plate reader (PerkinElmer).

Peripheral Blood Cell Isolation from Murine Blood:

Murine blood was obtained by terminal cardiac puncture and contained in heparin-coated tubes. Cells were isolated by density gradient centrifugation using Lympholyte-M (Cederlane Labs).

Peripheral Blood Cell Isolation from Human Blood:

20ml blood was collected from 25 healthy donors or 18 metastatic melanoma patients under protocol LCCC 1715 after written consent was obtained. Inclusion criteria for healthy cohort: 1. Healthy donors were older than 18 years of age. 2. Male or female. 3. No documented diagnosis of cancer. 3. Donors consented to providing a one-time blood sample of up to 20ml. 4. Consented to abstraction of their medical records as evidence by signed HIPPA form. 5. Signed institutional review board (IRB)-approved informed consent document. Inclusion criteria for melanoma cohort: 1. 18 years of age or older. 2. Male or Female. 3. English-speaking. 4. Appointment at the NC Cancer Hospital (NCCH) for treatment of a pathologically or diagnostically confirmed diagnosis of metastatic melanoma. 5. Patient consented to providing a baseline blood sample of up to 20ml. 6. Consents to abstraction of their medical records as evidence by signed HIPPA form for this protocol. 7.

Signed an institutional review board (IRB)-approved informed consent document for this protocol. Exclusion criteria for both cohorts: 1. Younger than 18 years of age. 2. Dementia, altered mental status, or any psychiatric condition that would prohibit the understanding or rendering of informed consent. 3. Diagnosis of autoimmune diseases, or chronic or acute infection. 4. Non-English speaking. Cells were immediately isolated by density gradient centrifugation using Lympholyte-poly (Cederlane Labs, CL5071) then stained for flow cytometry analysis.

MDSC-mediated T Cell Suppression Assay:

Assay adapted from (44). Spleens and lymph nodes were harvested from OT-I mice (C57BL/6-Tg(TcraTcrb)1100Mjb/J, Jackson Labs) and homogenized by pushing cells through a 70μM mesh strainer with a syringe plunger. Red blood cells were lysed using Red Blood Cell Lysis Buffer (Sigma-Aldrich, R7757). Splenocytes were stained with Cell Proliferation Dye eFluor 450 (eBioscience, 65–0842-85) according to manufacturer's protocol. Briefly, splenocytes were stained with 10μM dye in the dark at room temperature for 20 minutes. Serum-containing RPMI was added to quench the reaction on ice for 5 minutes. Stained splenocytes were incubated with FACS sorted MDSCs at a 1:1 ratio in a 96-well v-bottom plate (Costar, 3894). Proliferation was stimulated with OVA-257 (SIINFEKL) peptide (Sigma-Aldrich) at a final concentration of 1μg/ml. Influenza peptide was used as an irrelevant peptide negative control. Cells were incubated in a tissue culture incubator at 37°C for 5 days. Dye dilution was measured by flow cytometry on a BD LSR Fortessa using FACS Diva.

ELISPOT:

FACS sorted MDSCs and OT-I splenocytes were incubated at a 1:1 ratio on ELISPOT plates, stimulated with OVA-257 or an influenza peptide control and incubated for 5 days in a tissue culture incubator at 37°C. Mouse IFN-γ ELISpot (MABTECH) was performed according to manufacturer's guidelines. Briefly, cells were incubated in an antibody-coated plate for 48 hours in a tissue culture incubator at 37°C. Cells were then removed and detection antibody was added and the plate incubated for 2 hours at room temperature. Streptavidin-HRP was added after the plate was washed and incubated for 1 hour at room temperature. The plate was washed and substrate solution was added for 10 minutes until spots developed at room temperature. The plate was then washed in deionized water. Spots were imaged and quantified using an Elispot Reader System (AID, Autoimmun Diagnostika GMBH).

Differentiation Assay:

In vitro: FACS sorted MDSCs were incubated in a tissue culture incubator at 37°C with 5% CO_2 with 10ng/ml GM-CSF (R&D Systems) for 3 days then stained for 1 hour at room temperature in the dark and analyzed by flow cytometry on a BD LSR Fortessa using FACS Diva for markers of dendritic cells (CD11c$^+$MHCII$^+$) and macrophages (CD11b$^+$F4/80$^+$).

In vivo: FACS sorted MDSCs were stained with eFluor 450 proliferation dye then implanted into mice with tumor cells at a 1:10 MDSC:tumor cell ratio. Mice were euthanized and tumors were resected 3 days later and eFluor 450 proliferation dye positive cells were

analyzed by flow cytometry for markers of dendritic cells (CD11c$^+$MHCII$^+$) and macrophages (CD11b$^+$F4/80$^+$).

MDSC Migration Assay:

FACS sorted MDSCs were stained with eFluor 450 proliferation dye then implanted into the right flank of mice with tumor cells at a 1:10 MDSC:tumor cell ratio. Mice were euthanized and tumors and tumor-draining lymph nodes were resected 72 hours later and analyzed by flow cytometry for eFluor 450 proliferation dye positive cells.

Bone marrow-derived MDSCs:

BM-MDSCs were derived as previously described (45). Briefly, bone marrow was harvested and incubated in a tissue culture incubator at 37°C with 5% CO_2 for 5 days with 40ng/ml GM-CSF, 40ng/ml G-CSF and 40ng/ml IL-6 in RPMI with fetal bovine serum. Media and cytokines were replaced every 3 days.

Antibodies:

Flow cytometry - mouse: CD11b (BD Biosciences 562605), Ly6C (BD Biosciences 561237), Ly6G (BD Biosciences 563978), Mer (Biolegend 151506), Axl (R&D Systems FAB8541A), Tyro3 (R&D Systems FAB759G), F4/80 (BD Biosciences 123141), CD11c (BD Biosciences 564080), MHC II (BD Biosciences 743872), CD8 (Miltenyi Biotec 130–109-250), CD45 (BD Biosciences564279). Flow cytometry – human: CD11b (BD Biosciences 562723), CD14 (Miltenyi Biotec 130–110-521), CD15 (Miltenyi Biotec 130–104-939), CD66b (BD Biosciences 561927), HLA DR (BD Biosciences 565972), CD33 (BD Biosciences 563171), Lineage Cocktail (Biolegend 348807), Mer (Biolegend 367603), Axl (R&D Systems FAB154A), Tyro3 (R&D Systems FAB859P), CD16 (BD Biosciences 564434). Western blot: p-Stat3 (Cell Signaling 49081), Stat3 (Cell Signaling 9139), Actin (Cell Signaling 3700), N14 (Rockland scientific). Immunoprecipitation: MERTK (Invitrogen 14–5751-82). Immunofluorescence: Stat3 (Abnova PAB6030).

Immunoprecipitation:

Cells were lysed in coimmunoprecipitation (co-IP) lysis buffer (20 mM Hepes, 2 mM EDTA, 10 mM NaF, 150 mM NaCl, 10% glycerol, 0.5% Nonidet P-40) containing 1 tablet each of protease and phosphatase inhibitors (Roche, Complete protease inhibitor cocktail 11697498001, PhosSTOP 4906845001)and lysates were precleared by centrifuging at 10,000rpm for 30 minutes at 4°C. Lysates were incubated with PA/GS beads (Santa Cruz Biotechnology, sc-2003) and the appropriate primary antibody on a rotator overnight at 4°C. Immunoprecipitates were washed 3 times in co-IP lysis buffer and subjected to Western blot analysis. Briefly, proteins were resolved by SDS-PAGE and transferred to a PVDF membrane and incubated overnight at 4°C with the indicated antibody. Blots were developed using ECL (Pierce, 34095) and imaged on a BioRad Imaging System (BioRad ChemiDoc XRS+).

Immunofluorescence microscopy:

MDSCs were plated on slides then fixed with 4% paraformaldehyde and permeabilized with 0.1% Triton-X 100. These slides were blocked in 5% BSA dissolved in PBS, incubated with primary antibodies at a 1:500 dilution in PBS with BSA, washed with PBS with BSA, and incubated with secondary antibodies at a 1:500 dilution. After another wash with PBS with BSA, the slides were mounted in Prolong gold (Invitrogen-Life Technologies, P36930). Immunofluorescently labeled cells were imaged using an LSM 710 Spectral Confocal Laser Scanning Microscope (Zeiss). 15 independent images for each treatment were obtained and colocalization analysis of the confocal images was performed using ImageJ software (NIH).

Reagents:

STAT3 inhibitor NSC 74859 (Selleckchem S1155) was dissolved in DMSO, STAT3 activator Colivelin (Tocris 3945) was dissolved in 20% ethanol in water, p38 MAPK Inhibitor XIX Skepinone-L (Calbiochem 506174) was dissolved in DMSO, ERK Inhibitor II (Millipore Sigma 328007) was dissolved in DMSO, JNK Inhibitor VIII (Millipore Sigma 420135) was dissolved in DMSO. 1μM of each inhibitor was added to cells in RPMI with FBS and incubated for 2 hours in a tissue culture incubator with 5% CO_2 at 37°C.

MTS Assay:

$BRAF^{V600E}PTEN^{-/-}$ cells were incubated with the indicated concentration of the TYRO3, AXL, and MERTK inhibitor UNC4241 for 24, 48 or 72 hours. The MTS assay was performed by adding 20μl CellTiter reagent and incubating the plate for 4 hours in a tissue culture incubator with 5% CO_2 at 37°C (Cell Titer, Promega, G3582). Absorbance was then read at 490nm.

Immunohistochemistry:

IHC for CD8 was performed by the Animal Histopathology & Laboratory Medicine Core at the University of North Carolina, which is supported in part by an NCI Center Core Support Grant (5P30CA016086–41) to the UNC Lineberger Comprehensive Cancer Center. Briefly, immunohistochemical analysis for was performed on 4 micron thick paraffin sections on the Roche DISCOVERY Ultra automated platform. Automated antigen retrieval was performed using CC1, pH 8.5 (Roche, 950–124) for 64 minutes at 100° Celsius. The CD8a primary antibody (Cell Signaling, 98941, CD8α (D4W2Z) XP® Rabbit mAb (Mouse Specific)) was incubated for 2 hours at room temperature at a final dilution of approximately 1:400 titrated in DISCOVERY PSS Diluent (Roche, 760–212). This was followed by a post-primary hydrogen peroxidase incubation for 32 minutes, secondary antibody (DISCOVERY OmniMap anti-Rabbit HRP, ready-to-use dilution, Roche 760–4311) for 32 minutes, DISCOVERY Purple chromagen (Roche, 760–229) for 32 minutes, hematoxylin II (Roche, 790–2208) for 12 minutes, and bluing reagent (Roche,760–2037) for 4 minutes, all at room temperature.

The Translation Pathology Lab (TPL) scanned tissue sections stained for single target detection of CD8 on the ScanScope XT (Leica Biosystems) with a 20X power Olympus UPlanSApo objective. Exposure times were set according to the calibration data from the line camera. The output was in the format of ScanScope Virtual Slide (.svs) files saved with

8-bit image depth and JPEG2000 compression (compression quality set to 70). The ScanScope XT uses a halogen light source (TechniQuip).

Quantification and Statistical Analysis:

Specific statistical tests are reported in the Fig. Legends. GraphPad Prism 6 was used for all statistical analyses. Unpaired two-tailed t-test were used to compare mean differences between control and treatment groups. Mann Whitney tests were used for human data analysis. A p-value of less than 0.05 was considered significant.

Synthesis of UNC4241:

See Supplemental Figure 3A–B for schematic.

***trans*-4-((5-bromo-2-((4-Fluorophenyl)amino)pyrimidin-4-yl)amino)cyclohexan-1-ol (2)**—To a suspension of **1** (30.6 g, 100 mmol) and 4-fluoroaniline (14.1 mL, 150 mmol) in acetonitrile (350 mL) was added a 4.0 M HCl solution in 1,4-dioxane (90 mL, 360 mmol). The resulting mixture was heated at 82 °C (under reflux) overnight. After cooled to room temperature, the suspension was filtered, and the precipitate was washed with CH_2Cl_2 (2X). The filtrate was concentrated to provide the HCl salt of the desired compound **2** as a pale white solid (42 g, 100%). MS (ESI) for $[M+H]^+$ ($C_{16}H_{19}BrFN_4O^+$): calcd. m/z 381.06; found m/z 381.10.

***trans*-4-((5-(5-(1,3-Dioxolan-2-yl)pyridin-2-yl)-2-((4-fluorophenyl)amino)pyrimidin-4-yl)amino)cyclohexan-1-ol:** (**4**) A solution of **2** (6.6 g, 15.8 mmol) in dimethylformamide (DMF) (72 mL) was added an aqueous solution of K_2CO_3 (8.72 g in 24 mL water) at room temperature. The mixture was stirred vigorously in a three-neck flask equipped with a condenser opening to the air and was added **3** (10.38 g, 47.4 mmol). After stirring at room temperature for 5 minutes, the reaction mixture was added $PdCl_2(dppf) \cdot CH_2Cl_2$ (1.29 g, 1.58 mmol) and CuBr (452 mg, 3.16 mmol), stirred for another 2 to 3 minutes, then heated at 120 °C for 30 minutes in a pre-heated oil bath. The mixture was cooled to room temperature, then filtered through a pad of celite, and washed with DMF. The filtrate was concentrated under vacuum pressure. After drying under high vacuum for 30 minutes, the mixture was added CH_2Cl_2 and was sonicated for 1 hour. The precipitate was filtered with a Buchner glass funnel and provided the desired compound **4** (5.0 g, 70%) as a pale yellow solid.

6-(2-((4-Fluorophenyl)amino)-4-((*trans*-4-hydroxycyclohexyl)amino)pyrimidin-5-yl)nicotinaldehyde (5): **To** compound **4** (12.0 g, 26.6 mmol) in a round flask was added a 4 N HCl aqueous solution (300 mL). The mixture was heated at 100 °C (under reflux) for 3 hours, cooled to room temperature, then was poured into an ice-water bath. Sodium hydroxide (45.5 g, 1.14 mol) was added portion wise followed by potassium carbonate until the pH of the mixture was 8–9. The precipitated yellow solid was filtered to yield the desired compound **5** (6.7 g, 62%).

***trans*-4-((2-((4-Fluorophenyl)amino)-5-(5-(pyrrolidin-1-ylmethyl)pyridin-2-yl) pyrimidin-4-yl)amino)cyclohexan-1-ol (UNC4241A):** a suspension of **5** (6.6 g, 16.2

mmol) in CH_2Cl_2 (150 mL) was added pyrrolidine (2.6 mL, 32.4 mmol), sodium triacetoxyborohydride (6.87 g, 32.4 mmol), and acetic acid (1 mL, 17.5 mmol). The reaction mixture was stirred at room temperature overnight and then was added to pyrrolidine (1.3 mL, 16.2 mmol), sodium triacetoxyborohydride (3.44 g, 16.2 mmol) and acetic acid (0.5 mL, 8.7 mmol). After 2 h, the mixture was filtered. The filtrate was basified with a 1 M NaOH aqueous solution and then was extracted with a mixture of CH_2Cl_2 and MeOH (10:1) (3X). The combined organic layers were dried (using $MgSO_4$), concentrated and purified by column chromatography with ISCO system (0~10% MeOH in DCM+0.5% NH_3) to yield crude material, which was further purified by pre-HPLC on a reverse phase column (10~100% MeOH/water) to provide the TFA salt of the desired product. The TFA salt was dissolved in a 2 M HCl aqueous solution, sonicated for 30 min, and concentrated to yield the HCl salt of **UNC4241** (4.7 g, 51%) as an off-white solid. ^{1}H NMR (400 MHz, CD_3OD) δ 8.88 (s, 1H), 8.54 (s, 1H), 8.27 (d, J = 8.0 Hz, 1H), 8.10 (d, J = 8.2 Hz, 1H), 7.67 – 7.54 (m, 2H), 7.25 – 7.15 (m, 2H), 4.57 (s, 2H), 4.12 – 3.94 (m, 1H), 3.72 – 3.51 (m, 3H), 3.30 – 3.20 (m, 2H), 2.32 – 2.17 (m, 2H), 2.17 – 1.96 (m, 6H), 1.62 – 1.45 (m, 2H), 1.45 – 1.30 (m, 2H); ^{13}C NMR (101 MHz, CD_3OD) δ 163.16, 160.97, 160.72, 154.23, 152.20, 150.27, 142.77, 141.94, 133.74, 127.71, 126.36, 122.24, 116.95, 116.73, 107.41, 69.87, 55.74, 55.04, 51.83, 34.42, 30.53, 23.96; MS (ESI) for $[M+H]^+$ ($C_{26}H_{32}FN_6O^+$): calculated. m/z 463.26; found m/z 463.30.

Results.

TAM receptor and ligand expression in MDSCs were elevated in tumor bearing mice.

Knowing that the TAM RTKs regulate some innate immune cells, we investigated their role in MDSCs. First, we measured the effect of tumor growth on MDSC receptor and ligand expression. MDSCs were purified by fluorescence-activated cell sorting (FACS) from the spleen and *Tyro3*, *Axl*, and *Mertk* and ligand expression were compared in $BRAF^{V600E}PTEN^{-/-}$ tumor-bearing and non-tumor bearing mice. We observed dramatic increases in expression of all three receptors and the ligands in MDSCs from tumor-bearing mice (Fig. 1A). Next, we quantified the surface expression of TYRO3, AXL and MERTK MDSCs in non-tumor bearing mouse blood, and tumor bearing mouse blood and tumors. There was no change in Axl expression in the blood of control and tumor bearing mice but both MERTK and TYRO3 increased in M- and PMN-MDSCs in the blood of tumor bearing mice (Fig. 1B–C). All three receptors showed increased MDSC surface expression in the tumors compared to their level in the blood of the same animals (Fig. 1B–C).

To study the effect of each individual receptor, splenic (Supplemental Fig. S1A–B) and intratumoral (Fig. 1D and Supplemental Fig. S1C. Gating strategy in Supplemental Fig. S1D) MDSCs were isolated from WT, $Axl^{-/-}$, $Mertk^{-/-}$, and $Tyro3^{-/-}$ mice bearing syngeneic $BRAF^{V600E}PTEN^{-/-}$ tumors. The number of splenic MDSCs increased in the different knock-out mice bearing tumors by a small increment although the $Axl^{-/-}$ mouse showed a slight decrease in PMN-MDSCs (Supplemental Fig. S1B). In contrast, while the percentage of intratumoral M-MDSCs was similar in WT and $Axl^{-/-}$ mice, there was a decrease in $Mertk^{-/-}$ and $Tyro3^{-/-}$ mice suggesting a migration, homing or survival defect in moving to or surviving in the tumor in the absence of either MERTK or TYRO3 (Fig. 1D).

TYRO3, AXL and MERTK promoted MDSC immune suppressive function.

To test if TYRO3, AXL and MERTK alter the suppressive abilities of MDSCs, MDSCs from the spleens of WT, $Axl^{-/-}$, $Mertk^{-/-}$, and $Tyro3^{-/-}$ mice bearing BRAF^{V600E}PTEN$^{-/-}$ tumors were FACS purified and RNA was extracted for quantitative real-time PCR (qRT-PCR) analysis. Arginase 1, iNOS, TGF-β and IDO expression were substantially reduced in $Axl^{-/-}$, $Mertk^{-/-}$, and $Tyro3^{-/-}$ M-MDSCs (Fig. 2A–D). Arginase expression was significantly decreased in $Axl^{-/-}$, $Mertk^{-/-}$, and $Tyro3^{-/-}$ PMN-MDSCs, while TGF-β and IDO were more variable (Fig. 2C–D). ROS production, a major mechanism of PMN-MDSC activity, was measured enzymatically over 24 hours after isolation and found to be decreased in $Axl^{-/-}$, $Mertk^{-/-}$, and $Tyro3^{-/-}$ PMN-MDSCs compared to WT PMN-MDSCs (Fig. 2E). These findings indicate that absence of TYRO3, AXL or MERTK decrease the suppressive capabilities of MDSCs with a greater influence on M- than PMN-MDSCs.

To determine if $Axl^{-/-}$, $Mertk^{-/-}$ and $Tyro3^{-/-}$ MDSCs altered their ability to suppress CD8$^+$ T-cell proliferation, we performed *in vitro* antigen-specific T cell proliferation assays using the model antigen OVA and OVA specific T cells. $Axl^{-/-}$, $Mertk^{-/-}$ and $Tyro3^{-/-}$ M-MDSCs suppressed T cell proliferation less compared to WT MDSCs (Fig. 2F). Consistent with this finding, $Axl^{-/-}$, $Mertk^{-/-}$ and $Tyro3^{-/-}$ M-MDSCs allowed an enhancement in the generation of OVA antigen-specific T-cell responses based on IFN-γ ELISPOT assays (Supplemental Fig. S2A).

To determine if MDSC differentiation into more mature, less suppressive macrophages and DCs (42) was affected by TAM RTKs, we FACS sorted M-MDSCs from the spleens of tumor-bearing mice, incubated them with GM-CSF and analyzed cell surface markers by flow cytometry 5 days later. $Axl^{-/-}$, $Mertk^{-/-}$ and $Tyro3^{-/-}$ MDSCs differentiated to DCs (CD11c$^+$MHCII$^+$) (Fig. 2G and Supplemental Fig. S2B) and macrophages (CD11b$^+$F4/80$^+$) (Fig. 2G and Supplemental Fig. S2C) at a higher frequency than their WT counterparts. To investigate if this was only an *ex vivo* phenomenon, we subcutaneously implanted FACS-sorted MDSCs stained with e450 proliferation dye, serving as a marker to distinguish implanted MDSCs from naïve MDSCs, into mice along with BRAF^{V600E}PTEN$^{-/-}$ melanoma cells. 48 hours later the implanted e450 proliferation dye positive cells were analyzed for cell surface markers by flow cytometry. $Axl^{-/-}$, $Mertk^{-/-}$ and $Tyro3^{-/-}$ e450$^+$ cells each exhibited markers for DCs (CD11c$^+$MHCII$^+$) (Fig. 2H and Supplemental Fig. S2D) and macrophages (CD11b$^+$F4/80$^+$) (Fig. 2H and Supplemental Fig. S2E) at higher levels than WT. Taken together, these findings suggest TYRO3, AXL or MERTK maintain MDSC immaturity.

MDSCs are actively recruited to tumor sites by chemokines produced by the tumor. To test whether $Mertk^{-/-}$ and $Tyro3^{-/-}$ MDSCs have a general migratory or homing defect, we FACS sorted MDSCs from WT and $Axl^{-/-}$, $Mertk^{-/-}$ and $Tyro3^{-/-}$ knock out mice and stained them with e450 proliferation dye. We mixed these MDSCs with BRAF^{V600E}PTEN$^{-/-}$ melanoma cells and implanted the mixture into WT mice and 72 hours later collected the tumors and tumor draining lymph nodes (TDLNs) and analyzed e450, CD11b, Ly6C and Ly6G to determine the proportion of MDSCs that remained in the tumor versus those that migrated to the (TDLN) using flow cytometry. $Mertk^{-/-}$ and $Tyro3^{-/-}$ MDSCs remained in the tumor while WT and $Axl^{-/-}$ MDSCs were more likely to migrate to the TDLN (Fig. 2I).

These results suggest that MERTK and TYRO3 influence MDSC migration from spleen to tumor and from tumor to TDLN - a major site of T cell activation or suppression.

To determine if $Axl^{-/-}$, $Mertk^{-/-}$ and $Tyro3^{-/-}$ MDSCs affect tumor growth, we FACS sorted WT, $Axl^{-/-}$, $Mertk^{-/-}$ and $Tyro3^{-/-}$ MDSCs and co-implanted them into the right flank with $BRAF^{V600E}PTEN^{-/-}$ melanoma cells in a 1:10 ratio (MDSC:tumor cells). Tumors were significantly smaller in mice receiving $Axl^{-/-}$, $Mertk^{-/-}$ and $Tyro3^{-/-}$ MDSCs compared to mice receiving WT MDSCs (Fig. 2J and Supplemental S2F). Thus, TYRO3, AXL and MERTK modulate and maintain MDSC suppressive function and $Axl^{-/-}$, $Mertk^{-/-}$ and $Tyro3^{-/-}$ MDSCs inhibit tumor growth, perhaps by creating a less suppressive TME.

Pan-TAM inhibitor UNC4241 inhibited MDSC capabilities and T cell suppression.

The above results suggest that AXL, MERTK and TYRO3 regulate MDSC activity to promote an immuno-tolerant microenvironment. To determine if inhibiting TYRO3, AXL and MERTK is therapeutically tractable, we employed UNC4241, a pan-TAM small molecule inhibitor with pharmacokinetic properties in mice allowing once daily dosing by oral gavage (IC_{50}: MERTK 1.4nM; AXL 5.4nM and TYRO3 2.3nM) (Supplemental Fig. S3A–B). MDSCs from tumor-bearing mice treated with vehicle or 25mg/kg UNC4241 for 3 weeks were FACS sorted and analyzed for their suppressive capabilities. UNC4241 reduced arginase 1 (Fig. 3A), iNOS (Fig. 3B) and IDO (Fig. 3D), while modestly lowering TGF-β expression (Fig. 3C) in M-MDSCs and ROS production (Fig. 3E) in PMN-MDSCs compared to vehicle treatment.

To test if UNC4241 alters the characteristics of MDSCs in a short-term *in vitro* assay, we cultured FACS sorted MDSCs with 300nM UNC4241 and assayed survival, differentiation and maintenance of Ly6C and Ly6G expression. UNC4241 had no effect on survival as measured by MTS assay (Supplemental Fig. S3C). In addition, we observed a slight increase in dendritic cell but not in macrophage differentiation (Supplemental Fig. S3D) and Ly6C and Ly6G levels were stable (Supplemental Fig. S3E).

To test if UNC4241 treatment mirrors the effect of *Axl*, *Mertk*, and *Tyro3* genetic deletion on T cell proliferation, we studied MDSC suppression of T cell proliferation in OVA-specific CD8 T cell proliferation assays. Purified MDSCs from tumor-bearing mice treated with UNC4241 for 3 weeks were isolated and incubated with splenocytes from OT-I mice. Compared to saline vehicle, UNC4241 treatment *in vivo* yielded MDSCs that were significantly less suppressive allowing increased T cell proliferation (Fig. 3F).

UNC4241 delayed tumor growth, promoted T cell infiltration and augmented anti-PD-1 therapy.

To test if UNC4241's reduction in MDSC suppression (Fig. 3) altered growth of $BRAF^{V600E}PTEN^{-/-}$ syngeneic melanoma *in vivo*, we subcutaneously injected cells and treated mice daily with UNC4241 for 5 weeks. While the cell line expresses all three RTKs (Supplemental Fig. S4A) UNC4241 did not inhibit proliferation *in vitro* (Supplemental Fig. S4B). In contrast, UNC4241 inhibited tumor growth compared to vehicle *in vivo* (Fig. 4A–B). To assess the UNC4241 immune consequences, immunohistochemistry (IHC) staining for CD8 was performed on fixed tumor sections; a greater than 4-fold increase in CD8 T cell

infiltration in UNC4241 treated tumors compared to vehicle treated (Fig. 4C) was observed. To determine if UNC4241 treatment increased dendritic cells and macrophages in tumors, we performed flow cytometry and found no change in dendritic cell frequency and a slight decrease in macrophage numbers in UNC4241 treated tumors (Fig. 4D and Supplemental Fig. S4D). To rule out a direct UNC4241 effect on CD8$^+$ T-cells, we performed *in vitro* T cell proliferation assays with CD8$^+$ T-cells pretreated with either vehicle or UNC4241 and found that CD8 T cell proliferation was unaffected (Supplemental Fig. S4C). To test if lessened MDSC suppression lead to the decrease in tumor growth, we repeated the tumor study with anti-Gr-1 antibody to deplete MDSCs. The antibody alone caused a non-significant reduction in tumor size whereas UNC4241 treated tumors were significantly smaller than control tumors. However, in the context of MDSC depletion with anti-Gr-1, UNC4241 no longer inhibited tumor growth (Fig. 4E).

To investigate if UNC4241 treatment augmented checkpoint inhibitor therapy, mice were injected with a BRAF^{V600E}PTEN$^{-/-}$ melanoma cell line and once tumors became palpable therapy was initiated with anti-PD-1 alone, UNC4241 alone, the combination of anti-PD-1 with UNC4241 or the vehicle treatment. While UNC4241 alone again decreased tumor growth, the combination of anti-PD-1 with UNC4241 significantly decreased tumor growth and prolonged survival with the median survival of anti-PD-1 alone being 75 days and combination anti-PD-1 and UNC4241 survival equaling 96 days (Fig. 4F–H).

TAMs facilitated MDSC action through Stat3 signaling.

To define mechanisms downstream of MERTK that maintain or enhance MDSC activity, we investigated pathways involved in MDSC biology that intersect with MERTK signaling, specifically STAT3 signaling (24). We analyzed STAT3 phosphorylation in MDSCs derived from bone-marrow precursors (BM-MDSCs) of WT and *Axl*$^{-/-}$, *Mertk*$^{-/-}$ and *Tyro3*$^{-/-}$ mice. STAT3 is activated by Tyr705 phosphorylation while transcriptional activation is regulated by Ser727 phosphorylation (46). The process of differentiating BM-MDSCs with cytokines (GM-CSF, G-CSF and IL-6) (45) resulted STAT3 Tyr705 phosphorylation in all four (WT, *Axl*$^{-/-}$, *Mertk*$^{-/-}$ and *Tyro3*$^{-/-}$) genotypes, presumably due to cytokine activation of JAK kinases (Fig. 5A). In contrast, STAT3 serine phosphorylation was markedly diminished in the *Axl*$^{-/-}$, *Mertk*$^{-/-}$ and *Tyro3*$^{-/-}$ MDSCs compared to WT (Fig. 5A). To investigate if the ligands GAS6 and Protein S induces STAT3 serine phosphorylation we treated BM-MDSCs with GAS6 or Protein S and evaluated STAT3 phosphorylation. While GAS6 induced serine phosphorylation in WT MDSCs, Protein S did not (Fig. 5B). Additionally, GAS6-dependent STAT3 serine phosphorylation was lost in *Axl*$^{-/-}$, *Mertk*$^{-/-}$ and *Tyro3*$^{-/-}$ MDSCs. To see if GAS6 or Protein S treatment induced complex formation between MERTK and STAT3, we treated BM-MDSCs and immunoprecipitated MERTK. Following GAS6 stimulation, STAT3 precipitated in a complex with MERTK and STAT3 exhibited increased serine phosphorylation, however we saw no effect with Protein S treatment (Fig. 5C). The increase in p-Ser STAT3 was inhibited by UNC4241 (Fig. 5C). Given the observed change in serine phosphorylation, we investigated serine kinases known to phosphorylate STAT3 that are downstream of MERTK. We determined that GAS6-dependent STAT3 serine phosphorylation was most inhibited by a p38 inhibitor, very modestly inhibited by a JNK inhibitor and not altered by an ERK inhibitor (Supplemental

Fig. S5A–C). We also demonstrated that GAS6-stimulated MERTK immunoprecipitated with both STAT3 and p38 (Supplemental Fig. S5A). In addition, we examined STAT3 cellular localization by immunohistochemistry and determined that GAS6-induced nuclear translocation of STAT3 is detectable at 40 minutes following GAS6 treatment (Fig. 5D). We then showed that STAT3 inhibition reversed the T cell suppressive capability of WT MDSC from tumor bearing mice (Fig. 5E). To show that STAT3 functions downstream of the TAM RTKs, we showed that pre-treating MDSCs with a STAT pathway activator, reversed the loss of suppression seen in $Axl^{-/-}$, $Mertk^{-/-}$ and $Tyro3^{-/-}$ MDSCs (Fig. 5F). The latter result indicates that TAM RTK's control of STAT3 in part regulates MDSC immunosuppression. We also demonstrated that iNOS (Fig. 5G) and arginase (Fig. 5H) expression was induced by GAS6 and inhibited by UNC4241.

The frequency of TAM RTK$^+$ MDSCs was increased in Metastatic Melanoma Patients.

Circulating MDSCs can be detected in cancer patients and the number of MDSCs negatively correlate with response to checkpoint inhibitor therapy (38,47–49). Given the potential for targeting TYRO3, AXL and MERTK in human disease, we studied their surface expression on the three major subclasses of human circulating MDSCs, M-MDSCs (CD33$^+$CD14$^+$HLA-DR$^{lo/-}$CD15$^-$), PMN-MDSCs (CD14$^-$CD11b$^+$CD66b$^+$) and e-MDSCs (Lin$^-$(CD3/14/15/19/56) HLA-DR$^-$CD33$^+$)(50). We obtained blood from healthy donors and metastatic melanoma patients (IRB protocol LCCC 1715), isolated PBMCs and analyzed by an eleven-color flow assay to assess TAM RTK$^+$ MDSCs (gating strategy Supplemental Fig. S6A). We observed an increase in circulating MDSCs in melanoma patients versus healthy donors (Fig. 6A). There were more MERTK$^+$ MDSCs (20–50%) than AXL$^+$ or TYRO3$^+$ MDSCs (<2%) (Fig. 6B–D and Supplemental Fig. S6B–D). The relative MERTK$^+$ MDSC numbers increased in all three MDSC populations in melanoma patients. The relative increase of TYRO3$^+$ and AXL$^+$ M- and PMN-MDSCs are somewhat greater than those of MERTK$^+$ MDSCs but the absolute levels are considerably lower (Fig. 6B–D and Supplemental Fig. S6B–D). Intriguingly the percent increase in MERTK$^+$ early stage MDSCs is the greatest of the three subtypes (>10-fold) reaching 50% of the e-MDSCs (Fig. 6D and Supplemental Fig.6D). The percent increase in TYRO3$^+$ MDSCs of all three subtypes is also noteworthy (>10-fold) but there are fewer than in the MERTK$^+$ subset. Taken together, these data suggest that the MERTK$^+$ MDSCs may serve as a marker of malignancy and potentially be a biomarker for response to therapy with MERTK inhibitors or other agents targeting the immune system.

Discussion.

This manuscript demonstrated that the innate immune RTKs, TYRO3, AXL and MERTK regulated MDSC suppressive activity in a STAT3 dependent manner and inhibition of TAM RTKs induced more robust anti-tumor responses. Receptor and ligand levels were increased on MDSCs in tumor-bearing mice compared to non-tumor bearing and that this RTK family regulated arginase 1, iNOS, IDO, TGF-β and ROS suppressive mechanisms. The absence of TAM RTKs inhibited MDSC migration and allowed differentiation to less suppressive mature cells. By using a pan-TAM inhibitor, UNC4241, we decreased melanoma tumor growth alleviating MDSC suppression, promoting greater T cell infiltration and augmenting

anti-PD-1 activity. Lastly, we found that MERTK, AXL and TYRO3 were upregulated on MDSCs in human melanoma patients.

Malignancies promote signaling networks leading to accumulation of MDSCs and their pathological action. (32,42). Tumor-bearing mice had more AXL^+, $MERTK^+$ and $TYRO3^+$ MDSCs compared to WT. Similarly, melanoma patients had an increase in $TYRO3^+$, AXL^+ and particularly $MERTK^+$ MDSCs compared to healthy donors. These data suggest that malignancy (and perhaps other inflammatory and cytokine producing conditions) induces TYRO3, AXL and MERTK expression on MDSCs helping to establish a suppressive TME and resistance to anti-cancer therapeutics.

MDSCs suppress T-cell activity through ROS, iNOS, arginase, IDO and TGF-β activity (51). Our data demonstrated that loss of either MERTK, TYRO3 or AXL down regulated arginase 1 expression in both M- and PMN-MDSCs while decreasing iNOS and ROS production. These results were recapitulated by receptor kinase inhibition with UNC4241. Downregulation of IDO and TGF-β by genetic deletion and drug inhibition was more striking in M-MDSCs and was variable in PMN-MDSCs. We demonstrated that MDSC-mediated antigen-specific suppression of T cell proliferation and activation is reduced in $Axl^{-/-}$, $Mertk^{-/-}$ or $Tyro3^{-/-}$ MDSCs and is again recapitulated by UNC4241 inhibition of TAM RTKs. We observed an increase of $CD8^+$ T-cell infiltration into tumors in UNC4241 treated mice compared to vehicle treated mice. To confirm that UNC4241 acted on MDSCs suppression, we depleted MDSCs during UNC4241 treatment and showed a decreased response to UNC4241, indicating that in this *in vivo* model UNC4241's method of action is primarily on MDSCs. To complement our depletion study, we co-implanted $Axl^{-/-}$, $Mertk^{-/-}$ or $Tyro3^{-/-}$ MDSCs with melanoma cells. Compared to tumors receiving WT MDSCs, tumors receiving null MDSCs were significantly smaller, suggesting that the lack of TYRO3, AXL or MERTK in MDSCs provided a less favorable environment for tumor growth. Taken together, these data demonstrate that the lack of TAM RTKs enhance the anti-tumor T cell response by reversing MDSC-mediated suppression and that the TAM RTKs are regulators of multiple suppression mechanisms.

While the precise differences between the TAM RTKs' roles and intracellular pathways need further investigation, it is clear that they are not redundant. It remains somewhat surprising that deletion of any one of the three family members results in similar deficits. Previous reports indicate that the loss of any of the TAM RTKs leads to defects in platelet aggregation (52). We observed some differences between these receptors in MDSCs, for example, MERTK and TYRO3 deletion produces a deficit in MDSC egress from the tumor to the TDLN, whereas AXL deletion does not. There are several possible explanations for this phenomenon, including that each receptor has a non-overlapping function. Another possibility is that not only may heterodimerization be important, but large oligomers of TAM RTKs may be required to optimally amplify the ligand-phosphatidyl serine suppressive signal. Since this phenomenon has now been observed in several signaling models (platelets (52), MDSCs (this work) and macrophages (29)), the mechanism will require further elucidation.

Emerging research indicates that intratumoral MDSCs are much more suppressive than MDSCs in lymphoid organs (53). Thus, preventing MDSCs from accumulating in the TME would potentially lessen the suppressive TME, and potentially enhance anti-tumor therapies. *Mertk*$^{-/-}$ and *Tyro3*$^{-/-}$ MDSCs do not migrate to or survive as well in the TME, thereby lessening the MDSC contribution to the suppressive TME. This suggests that TAM RTK inhibition could augment immunotherapy by decreasing MDSC accumulation in the TME.

Another area of research focuses on promoting MDSC differentiation into less suppressive, mature myeloid cells. MDSCs differentiate into DCs and macrophages and a number of studies focus on drug treatment to promote maturation (17). Among others, all-*trans* retinoic acid (ATRA) and vitamin D promote myeloid differentiation and have been studied in the context of MDSC maturation, however clinical trials have shown limited success (54,55). Our data also show that WT MDSCs are less able to differentiate into macrophages or dendritic cells, whereas loss of any single TAM RTK allows for more efficient differentiation, adding another mechanism through which TAM RTK inhibition can lessen immunosuppression and potentially augment responses to current standard of care therapies.

Consistent with TAM RTK knock-out MDSCs' ability to differentiate more easily is the loss of STAT3 serine phosphorylation in these cells. STAT3 regulates differentiation status in MDSCs and the loss of STAT3 gene expression allows for MDSC differentiation into DCs and macrophages (40). Therapeutic response may be linked to MDSCs differentiating to less suppressive myeloid cells. This suggests aiding differentiation via TAM RTK inhibition may one mechanism to enhance T cell-centric therapies.

STAT3 dimerization, nuclear translocation and DNA binding properties are initiated by phosphorylation at Tyr705, transcriptional activation is dependent on Ser727 phosphorylation through MAP Kinase family members (46). The ability to induce STAT3 serine phosphorylation with GAS6 treatment correlated with the induction of iNOS and Arginase RNA expression, events that were inhibited with UNC4241. A STAT3 inhibitor reduced MDSC suppression of T cell proliferation in WT MDSCs, while a STAT3 activator in TAM RTK null MDSCs bypassed the TAM RTK-dependency and restored MDSC suppression back to WT levels. These findings strongly indicate that TAM RTKs regulate various MDSC suppressive and anti-differentiation mechanisms in part through TAM RTK-dependent STAT3 signaling. The TAM RTKs' ability to regulate multiple aspects of MDSC suppression is significant as it suggests the TAM RTKs function as a myeloid checkpoint and that inhibition of this checkpoint could function as a switch, effectively "turning off" MDSC suppression. Interestingly, Protein S had no effect on STAT3 phosphorylation suggesting Gas6 and Protein S have non-redundant context specific signaling roles and to fully appreciate the complexity of innate immune activity the differential signaling aspects of these ligands need to be explored further.

While checkpoint inhibitor therapy is somewhat successful in melanoma patients, many do not exhibit long term survival due to initial or acquired resistance (56,57). A large effort is focused on determining mechanisms of resistance and combination therapies subverting resistance. Circulating MDSC levels are increased in cancer patients (39,47,48), negatively correlate with response to anti-PD-1 and anti-CTLA4 therapy (38,49) and correlate

Author Manuscript

negatively with patients' overall survival (58). Targeting MDSCs in human cancer is an intriguing thought and being actively investigated (51,55). Consistent with our murine data, we demonstrate that TAM RTKs are expressed at higher levels in human cancer patients compared to healthy donors. The data presented here suggest that elevated TAM RTK levels on MDSCs can be a potential biomarker and therapeutic target in patients. We demonstrated that inhibiting TAM RTKs with UNC4241 works on the myeloid compartment and augments T cell directed therapy. These and other data advocate for manipulating both the innate and adaptive immune systems to provide a more efficacious and durable anti-tumor immune response.

Supplementary Material

Refer to Web version on PubMed Central for supplementary material.

Acknowledgements.

References.

1. Thomas NE, Busam KJ, From L, Kricker A, Armstrong BK, Anton-Culver H, et al. Tumor-infiltrating lymphocyte grade in primary melanomas is independently associated with melanoma-specific survival in the population-based genes, environment and melanoma study. Journal of clinical oncology : official journal of the American Society of Clinical Oncology 2013;31(33): 4252–9 doi 10.1200/JCO.2013.51.3002. [PubMed: 24127443]

2. Herschkowitz JI, Zhao W, Zhang M, Usary J, Murrow G, Edwards D, et al. Comparative oncogenomics identifies breast tumors enriched in functional tumor-initiating cells. Proc Natl Acad Sci U S A 2012;109(8):2778–83 doi 10.1073/pnas.1018862108. [PubMed: 21633010]

3. Kawai O, Ishii G, Kubota K, Murata Y, Naito Y, Mizuno T, et al. Predominant infiltration of macrophages and CD8(+) T Cells in cancer nests is a significant predictor of survival in stage IV nonsmall cell lung cancer. Cancer 2008;113(6):1387–95 doi 10.1002/cncr.23712. [PubMed: 18671239]

4. Pitt JM, Vetizou M, Daillere R, Roberti MP, Yamazaki T, Routy B, et al. Resistance Mechanisms to Immune-Checkpoint Blockade in Cancer: Tumor-Intrinsic and -Extrinsic Factors. Immunity 2016;44(6):1255–69 doi 10.1016/j.immuni.2016.06.001. [PubMed: 27332730]

5. Zhao X, Subramanian S. Intrinsic Resistance of Solid Tumors to Immune Checkpoint Blockade Therapy. Cancer research 2017;77(4):817–22 doi 10.1158/0008-5472.CAN-16-2379. [PubMed: 28159861]

6. Hodi FS, O'Day SJ, McDermott DF, Weber RW, Sosman JA, Haanen JB, et al. Improved survival with ipilimumab in patients with metastatic melanoma. The New England journal of medicine 2010;363(8):711–23 doi 10.1056/NEJMoa1003466. [PubMed: 20525992]

7. Hamid O, Robert C, Daud A, Hodi FS, Hwu WJ, Kefford R, et al. Safety and tumor responses with lambrolizumab (anti-PD-1) in melanoma. The New England journal of medicine 2013;369(2):134–44 doi 10.1056/NEJMoa1305133. [PubMed: 23724846]

8. Stewart TJ, Smyth MJ. Improving cancer immunotherapy by targeting tumor-induced immune suppression. Cancer metastasis reviews 2011;30(1):125–40 doi 10.1007/s10555-011-9280-5. [PubMed: 21249424]

9. Gajewski TF, Schreiber H, Fu YX. Innate and adaptive immune cells in the tumor microenvironment. Nat Immunol 2013;14(10):1014–22 doi 10.1038/ni.2703. [PubMed: 24048123]

10. Vonderheide RH, Glennie MJ. Agonistic CD40 antibodies and cancer therapy. Clin Cancer Res 2013;19(5):1035–43 doi 10.1158/1078-0432.CCR-12-2064. [PubMed: 23460534]

11. Moran AE, Kovacsovics-Bankowski M, Weinberg AD. The TNFRs OX40, 4–1BB, and CD40 as targets for cancer immunotherapy. Curr Opin Immunol 2013;25(2):230–7 doi 10.1016/j.coi. 2013.01.004. [PubMed: 23414607]

12. Goldberg MV, Drake CG. LAG-3 in Cancer Immunotherapy. Current topics in microbiology and immunology 2011;344:269–78 doi 10.1007/82_2010_114. [PubMed: 21086108]

13. Anderson AC. Tim-3: an emerging target in the cancer immunotherapy landscape. Cancer immunology research 2014;2(5):393–8 doi 10.1158/2326-6066.CIR-14-0039. [PubMed: 24795351]

14. Byrne WL, Mills KH, Lederer JA, O'Sullivan GC. Targeting regulatory T cells in cancer. Cancer research 2011;71(22):6915–20 doi 10.1158/0008-5472.CAN-11-1156. [PubMed: 22068034]

15. Noy R, Pollard JW. Tumor-associated macrophages: from mechanisms to therapy. Immunity 2014;41(1):49–61 doi 10.1016/j.immuni.2014.06.010. [PubMed: 25035953]

16. Coussens LM, Zitvogel L, Palucka AK. Neutralizing tumor-promoting chronic inflammation: a magic bullet? Science 2013;339(6117):286–91 doi 10.1126/science.1232227. [PubMed: 23329041]

17. Gabrilovich DI, Nagaraj S. Myeloid-derived suppressor cells as regulators of the immune system. Nat Rev Immunol 2009;9(3):162–74 doi 10.1038/nri2506. [PubMed: 19197294]

18. Schlecker E, Stojanovic A, Eisen C, Quack C, Falk CS, Umansky V, et al. Tumor-infiltrating monocytic myeloid-derived suppressor cells mediate CCR5-dependent recruitment of regulatory T cells favoring tumor growth. J Immunol 2012;189(12):5602–11 doi 10.4049/jimmunol.1201018. [PubMed: 23152559]

19. Gardner A, Ruffell B. Dendritic Cells and Cancer Immunity. Trends in immunology 2016;37(12): 855–65 doi 10.1016/j.it.2016.09.006. [PubMed: 27793569]

20. Veglia F, Gabrilovich DI. Dendritic cells in cancer: the role revisited. Curr Opin Immunol 2017;45:43–51 doi 10.1016/j.coi.2017.01.002. [PubMed: 28192720]

21. Mullard A Immunotherapy interest drives IDO deals. Nature Reviews Drug Discovery 2015;14:373.

22. Kaneda MM, Messer KS, Ralainirina N, Li H, Leem CJ, Gorjestani S, et al. PI3Kgamma is a molecular switch that controls immune suppression. Nature 2016;539(7629):437–42 doi 10.1038/nature19834. [PubMed: 27642729]

23. De Henau O, Rausch M, Winkler D, Campesato LF, Liu C, Cymerman DH, et al. Overcoming resistance to checkpoint blockade therapy by targeting PI3Kgamma in myeloid cells. Nature 2016;539(7629):443–7 doi 10.1038/nature20554. [PubMed: 27828943]

24. Graham DK, DeRyckere D, Davies KD, Earp HS. The TAM family: phosphatidylserine sensing receptor tyrosine kinases gone awry in cancer. Nature reviews Cancer 2014;14(12):769–85. [PubMed: 25568918]

25. Lemke G, Rothlin CV. Immunobiology of the TAM receptors. Nat Rev Immunol 2008;8(5):327–36 doi 10.1038/nri2303. [PubMed: 18421305]

26. Geng K, Kumar S, Kimani SG, Kholodovych V, Kasikara C, Mizuno K, et al. Requirement of Gamma-Carboxyglutamic Acid Modification and Phosphatidylserine Binding for the Activation of Tyro3, Axl, and Mertk Receptors by Growth Arrest-Specific 6. Front Immunol 2017;8:1521 doi 10.3389/fimmu.2017.01521. [PubMed: 29176978]

27. Lemke G Phosphatidylserine Is the Signal for TAM Receptors and Their Ligands. Trends Biochem Sci 2017;42(9):738–48 doi 10.1016/j.tibs.2017.06.004. [PubMed: 28734578]

28. Cummings CT, Deryckere D, Earp HS, Graham DK. Molecular pathways: MERTK signaling in cancer. Clin Cancer Res 2013;19(19):5275–80 doi 10.1158/1078-0432.ccr-12-1451. [PubMed: 23833304]

29. Ubil E, Caskey L, Holtzhausen A, Hunter D, Story C, Earp HS. Tumor-secreted Pros1 inhibits macrophage M1 polarization to reduce antitumor immune response. J Clin Invest 2018;128(6): 2356–69 doi 10.1172/JCI97354. [PubMed: 29708510]

30. Camenisch TD, Koller BH, Earp HS, Matsushima GK. A novel receptor tyrosine kinase, Mer, inhibits TNF-alpha production and lipopolysaccharide-induced endotoxic shock. J Immunol 1999;162(6):3498–503. [PubMed: 10092806]

31. Cook RS, Jacobsen KM, Wofford AM, DeRyckere D, Stanford J, Prieto AL, et al. MerTK inhibition in tumor leukocytes decreases tumor growth and metastasis. J Clin Invest 2013;123(8): 3231–42 doi 10.1172/jci67655. [PubMed: 23867499]

32. Veglia F, Perego M, Gabrilovich D. Myeloid-derived suppressor cells coming of age. Nat Immunol 2018;19(2):108–19 doi 10.1038/s41590-017-0022-x. [PubMed: 29348500]

33. Tcyganov E, Mastio J, Chen E, Gabrilovich DI. Plasticity of myeloid-derived suppressor cells in cancer. Curr Opin Immunol 2018;51:76–82 doi 10.1016/j.coi.2018.03.009. [PubMed: 29547768]

34. Ostrand-Rosenberg S, Fenselau C. Myeloid-Derived Suppressor Cells: Immune-Suppressive Cells That Impair Antitumor Immunity and Are Sculpted by Their Environment. J Immunol 2018;200(2):422–31 doi 10.4049/jimmunol.1701019. [PubMed: 29311384]

35. Goh C, Narayanan S, Hahn YS. Myeloid-derived suppressor cells: the dark knight or the joker in viral infections? Immunological reviews 2013;255(1):210–21 doi 10.1111/imr.12084. [PubMed: 23947357]

36. Ostrand-Rosenberg S, Sinha P, Figley C, Long R, Park D, Carter D, et al. Frontline Science: Myeloid-derived suppressor cells (MDSCs) facilitate maternal-fetal tolerance in mice. J Leukoc Biol 2017;101(5):1091–101 doi 10.1189/jlb.1HI1016-306RR. [PubMed: 28007981]

37. He YM, Li X, Perego M, Nefedova Y, Kossenkov AV, Jensen EA, et al. Transitory presence of myeloid-derived suppressor cells in neonates is critical for control of inflammation. Nat Med 2018 doi 10.1038/nm.4467.

38. Meyer C, Cagnon L, Costa-Nunes CM, Baumgaertner P, Montandon N, Leyvraz L, et al. Frequencies of circulating MDSC correlate with clinical outcome of melanoma patients treated with ipilimumab. Cancer immunology, immunotherapy : CII 2014;63(3):247–57 doi 10.1007/s00262-013-1508-5. [PubMed: 24357148]

39. Yu J, Du W, Yan F, Wang Y, Li H, Cao S, et al. Myeloid-derived suppressor cells suppress antitumor immune responses through IDO expression and correlate with lymph node metastasis in patients with breast cancer. J Immunol 2013;190(7):3783–97 doi 10.4049/jimmunol.1201449. [PubMed: 23440412]

40. Kumar V, Cheng P, Condamine T, Mony S, Languino LR, McCaffrey JC, et al. CD45 Phosphatase Inhibits STAT3 Transcription Factor Activity in Myeloid Cells and Promotes Tumor-Associated Macrophage Differentiation. Immunity 2016;44(2):303–15 doi 10.1016/j.immuni.2016.01.014. [PubMed: 26885857]

41. Zhao F, Xiao C, Evans KS, Theivanthiran T, DeVito N, Holtzhausen A, et al. Paracrine Wnt5a-beta-Catenin Signaling Triggers a Metabolic Program that Drives Dendritic Cell Tolerization. Immunity 2018;48(1):147–60 e7 doi 10.1016/j.immuni.2017.12.004. [PubMed: 29343435]

42. Youn JI, Nagaraj S, Collazo M, Gabrilovich DI. Subsets of myeloid-derived suppressor cells in tumor-bearing mice. J Immunol 2008;181(8):5791–802. [PubMed: 18832739]

43. Holtzhausen A, Zhao F, Evans KS, Tsutsui M, Orabona C, Tyler DS, et al. Melanoma-Derived Wnt5a Promotes Local Dendritic-Cell Expression of IDO and Immunotolerance: Opportunities for Pharmacologic Enhancement of Immunotherapy. Cancer immunology research 2015;3(9):1082–95 doi 10.1158/2326-6066.CIR-14-0167. [PubMed: 26041736]

44. Bayne LJ, Vonderheide RH. A myeloid-derived suppressor cell-mediated T-cell suppression assay for functional evaluation of immune cells in tumor-bearing mice. Cold Spring Harbor protocols 2013;2013(9):849–53 doi 10.1101/pdb.prot077214. [PubMed: 24003206]

45. Marigo I, Bosio E, Solito S, Mesa C, Fernandez A, Dolcetti L, et al. Tumor-induced tolerance and immune suppression depend on the C/EBPbeta transcription factor. Immunity 2010;32(6):790–802 doi 10.1016/j.immuni.2010.05.010. [PubMed: 20605485]

46. Yu H, Lee H, Herrmann A, Buettner R, Jove R. Revisiting STAT3 signalling in cancer: new and unexpected biological functions. Nature reviews Cancer 2014;14(11):736–46 doi 10.1038/nrc3818. [PubMed: 25342631]

47. Marigo I, Dolcetti L, Serafini P, Zanovello P, Bronte V. Tumor-induced tolerance and immune suppression by myeloid derived suppressor cells. Immunological reviews 2008;222:162–79 doi 10.1111/j.1600-065X.2008.00602.x. [PubMed: 18364001]

48. Weide B, Martens A, Zelba H, Stutz C, Derhovanessian E, Di Giacomo AM, et al. Myeloid-derived suppressor cells predict survival of patients with advanced melanoma: comparison with regulatory T cells and NY-ESO-1- or melan-A-specific T cells. Clin Cancer Res 2014;20(6):1601–9 doi 10.1158/1078-0432.CCR-13-2508. [PubMed: 24323899]

49. Weber J, Gibney G, Kudchadkar R, Yu B, Cheng P, Martinez AJ, et al. Phase I/II Study of Metastatic Melanoma Patients Treated with Nivolumab Who Had Progressed after Ipilimumab. Cancer immunology research 2016;4(4):345–53 doi 10.1158/2326-6066.CIR-15-0193. [PubMed: 26873574]

50. Bronte V, Brandau S, Chen SH, Colombo MP, Frey AB, Greten TF, et al. Recommendations for myeloid-derived suppressor cell nomenclature and characterization standards. Nat Commun 2016;7:12150 doi 10.1038/ncomms12150. [PubMed: 27381735]

51. Gabrilovich DI. Myeloid-Derived Suppressor Cells. Cancer immunology research 2017;5(1):3–8 doi 10.1158/2326-6066.CIR-16-0297. [PubMed: 28052991]

52. Angelillo-Scherrer A, Burnier L, Flores N, Savi P, DeMol M, Schaeffer P, et al. Role of Gas6 receptors in platelet signaling during thrombus stabilization and implications for antithrombotic therapy. J Clin Invest 2005;115(2):237–46 doi 10.1172/JCI22079. [PubMed: 15650770]

53. Kumar V, Patel S, Tcyganov E, Gabrilovich DI. The Nature of Myeloid-Derived Suppressor Cells in the Tumor Microenvironment. Trends in immunology 2016;37(3):208–20 doi 10.1016/j.it.2016.01.004. [PubMed: 26858199]

54. Chesney JA, Mitchell RA, Yaddanapudi K. Myeloid-derived suppressor cells-a new therapeutic target to overcome resistance to cancer immunotherapy. J Leukoc Biol 2017;102(3):727–40 doi 10.1189/jlb.5VMR1116-458RRR. [PubMed: 28546500]

55. Tobin RP, Davis D, Jordan KR, McCarter MD. The clinical evidence for targeting human myeloid-derived suppressor cells in cancer patients. J Leukoc Biol 2017;102(2):381–91 doi 10.1189/jlb.5VMR1016-449R. [PubMed: 28179538]

56. Mellor AL, Munn DH. Creating immune privilege: active local suppression that benefits friends, but protects foes. Nat Rev Immunol 2008;8(1):74–80 doi 10.1038/nri2233. [PubMed: 18064049]

57. Sharma P, Hu-Lieskovan S, Wargo JA, Ribas A. Primary, Adaptive, and Acquired Resistance to Cancer Immunotherapy. Cell 2017;168(4):707–23 doi 10.1016/j.cell.2017.01.017. [PubMed: 28187290]

58. Lang S, Bruderek K, Kaspar C, Hoing B, Kanaan O, Dominas N, et al. Clinical Relevance and Suppressive Capacity of Human Myeloid-Derived Suppressor Cell Subsets. Clin Cancer Res 2018 doi 10.1158/1078-0432.CCR-17-3726.
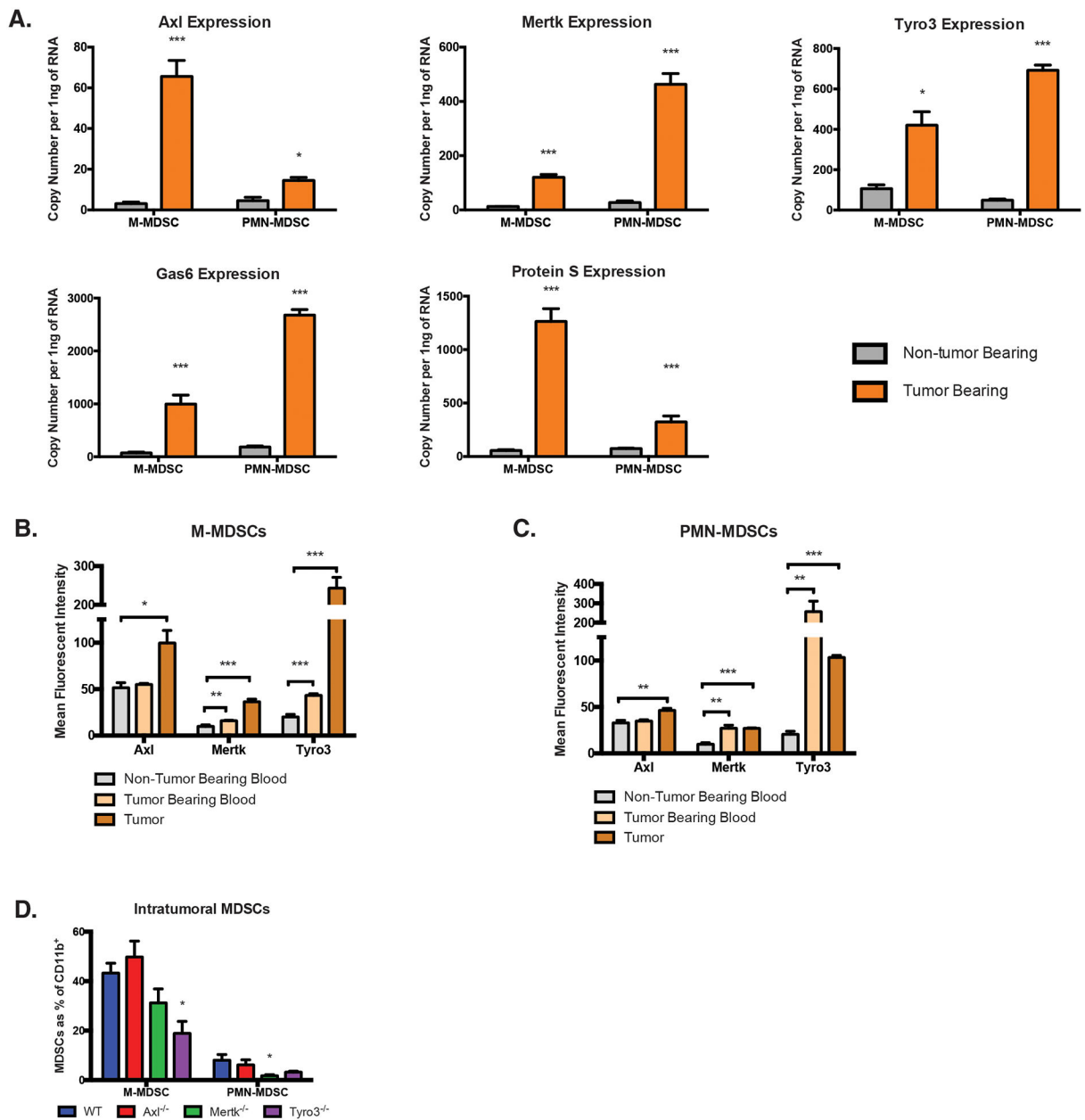
Figure 1: TAM receptor and ligand expression in MDSCs were elevated in tumor bearing mice.
A) qRT-PCR analysis of *Axl*, *Mertk*, *Tyro3* and ligands *Gas6* and *Protein S* in FACS sorted MDSCs from non-tumor bearing and tumor-bearing mice. n=5 *P<0.05 ***P<0.001. Quantification of AXL+, MERTK+ and TYRO3+ M-MDSCs (**B**) and PMN-MDSCs (**C**) in blood and tumors by flow cytometry. n=3 *P<0.05 **P<0.01 ***P<0.001. **D)** The percentage of M-MDSCs (CD11b+Ly6C+Ly6G−) and PMN-MDSCs (CD11b+Ly6intLy6G+) in tumors of tumor-bearing WT, *Axl*−/−, *Mertk*−/− and *Tyro3*−/− mice quantified by flow cytometry. n=5 *P<0.05 ***P<0.001. All data are mean ± SEM. Representative of 3 independent experiments. Significance calculated using the unpaired *t* test.
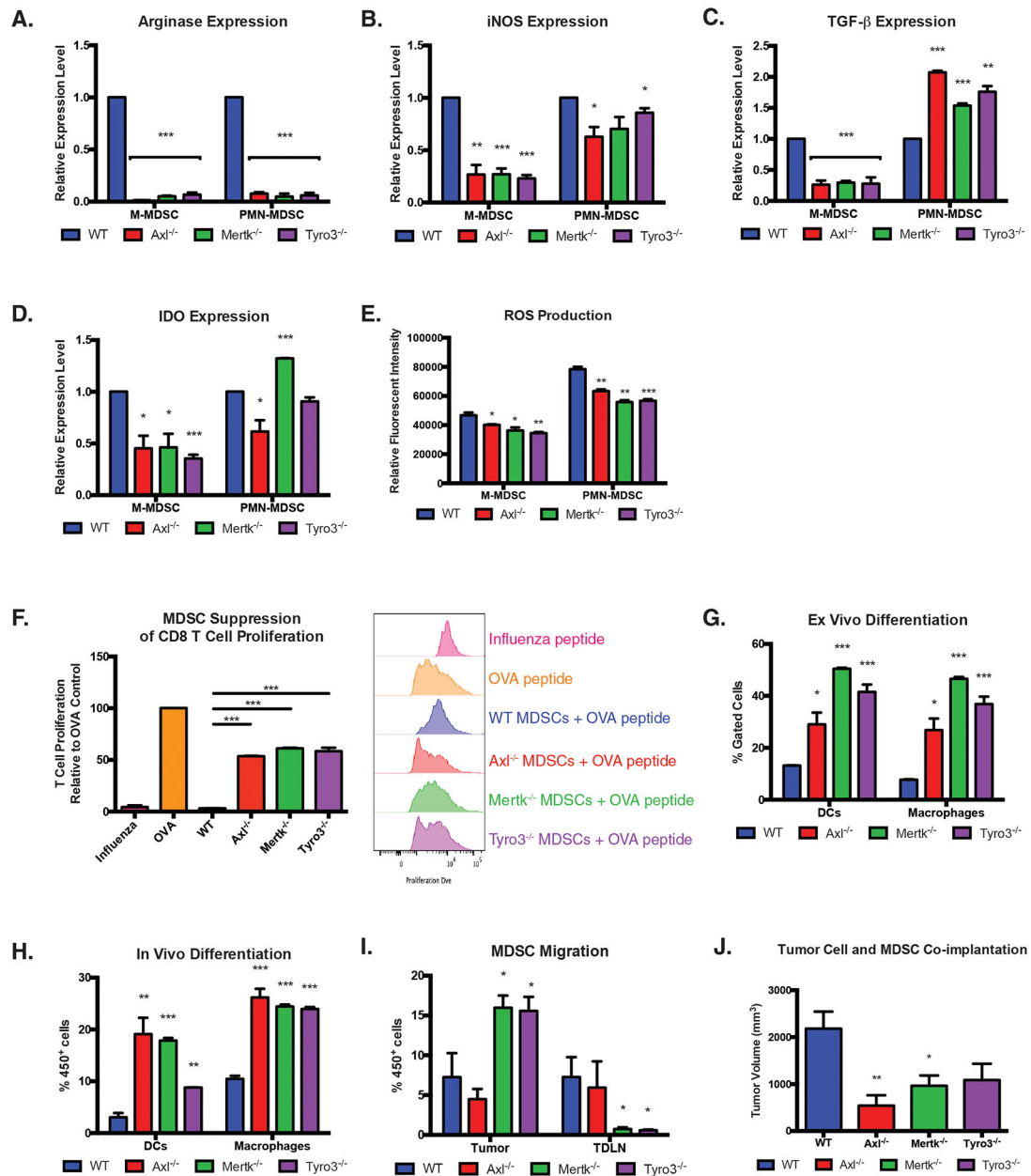
Figure 2: TYRO3, AXL and MERTK promoted MDSC immune suppressive function.
qRT-PCR analysis of Arginase (**A**), iNOS (**B**), TGF-β (**C**) and IDO (**D**) n=3 *P<0.05
P<0.01 ***P<0.001. **E) 2',7' –dichlorofluorescein (DCF) was measured with a
fluorescent plate reader as an output for reactive oxygen species (ROS) production.
Representative of 3 independent experiments. n=3 *P<0.05. **F)** WT, $Axl^{-/-}$, $Mertk^{-/-}$ and
$Tyro3^{-/-}$ MDSCs' suppression of OVA-stimulated CD8^{+} T-cell proliferation measured by
Cell Proliferation Dye eFluor 450 dilution. Normalized to OVA control. Representative of 2
independent experiments. n=3 for each experiment ***P<0.001. **G)** Flow cytometry analysis
of MDSCs incubated with GM-CSF for 3 days for markers of dendritic cells (CD11c
[+]MHCII^{+}) and macrophages (CD11b^{+}F4/80^{+}). Representative of 2 independent experiments.
n=3/group *P<0.05 ***P<0.001. **H)** eFluor 450 stained MDSCs implanted into mice with

tumor cells were resected 3 days after implantation and eFluor 450+ cells were analyzed for markers of dendritic cells (CD11c$^+$MHCII$^+$) and macrophages (CD11b$^+$F4/80$^+$). Representative of 2 independent experiments. n=3 **P<0.01 ***P<0.001. **I)** eFluor 450 stained MDSCs and tumor cells were implanted into mice. 72 hours later, tumors and tumor-draining lymph nodes (TDLN) were resected and eFluor 450+ cells were analyzed by flow for markers of dendritic cells (CD11c$^+$MHCII$^+$) and macrophages (CD11b$^+$F4/80$^+$) to asses implanted MDSCs' differentiation potential. Representative of 2 independent experiments. n=3 *P<0.05. **J)** BRAF^{V600E}PTEN$^{-/-}$ tumor cells and WT, *Axl$^{-/-}$*, *Mertk$^{-/-}$* or *Tyro3$^{-/-}$* MDSCs were implanted at a 1:10 MDSC:tumor ratio. Tumor volumes at day 19 post-implantation. n=5 *P<0.05 **P<0.01. All data are mean ± SEM. Significance calculated using the unpaired *t* test.
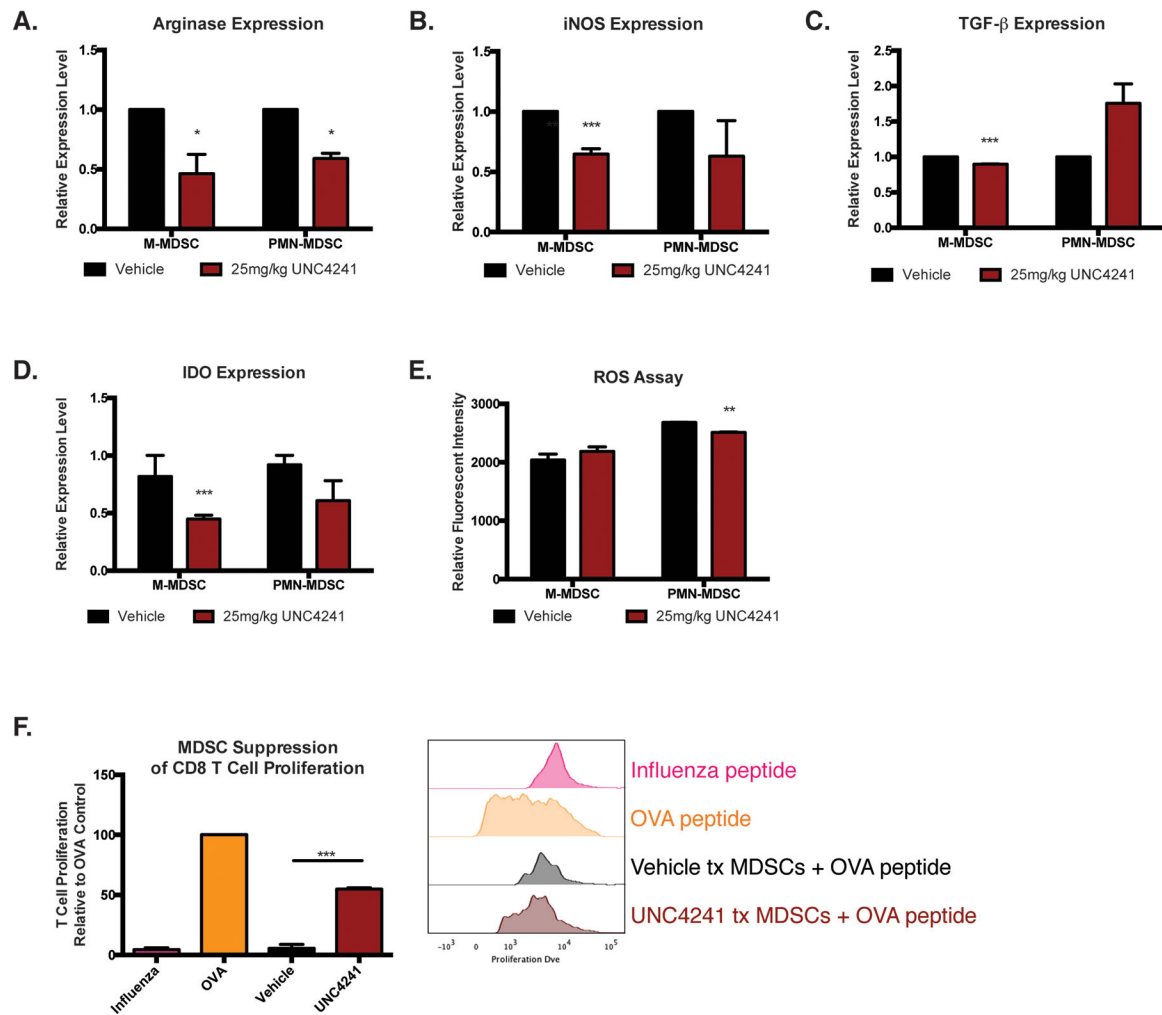
Figure 3: Pan-TAM inhibitor UNC4241 inhibited MDSC capabilities and T cell suppression.
qRT-PCR analysis on MDSCs FACS sorted from tumor-bearing mice treated with a saline
vehicle or 25mg/kg UNC4241 daily for arginase (**A**), iNOS (**B**), TGF-β (**C**) and IDO (**D**)
n=3 *P<0.05 **P<0.01 ***P<0.001. **E)** 2',7'-dichlorofluorescein (DCF) was measured with
a fluorescent plate reader as an output for reactive oxygen species (ROS) production.
Representative of 3 independent experiments. n=3 **P<0.01. **F**) FACS sorted MDSCs from
saline vehicle or UNC4241 treated mice were incubated with OVA-treated splenocytes from
OT-I mice and CD8$^+$ T-cell proliferation measured by Cell Proliferation Dye eFluor 450
dilution. Results were normalized to OVA control. Representative of 2 independent
experiments. n=3/group ***P<0.001. All data are mean ± SEM. Significance calculated
using the unpaired *t* test.

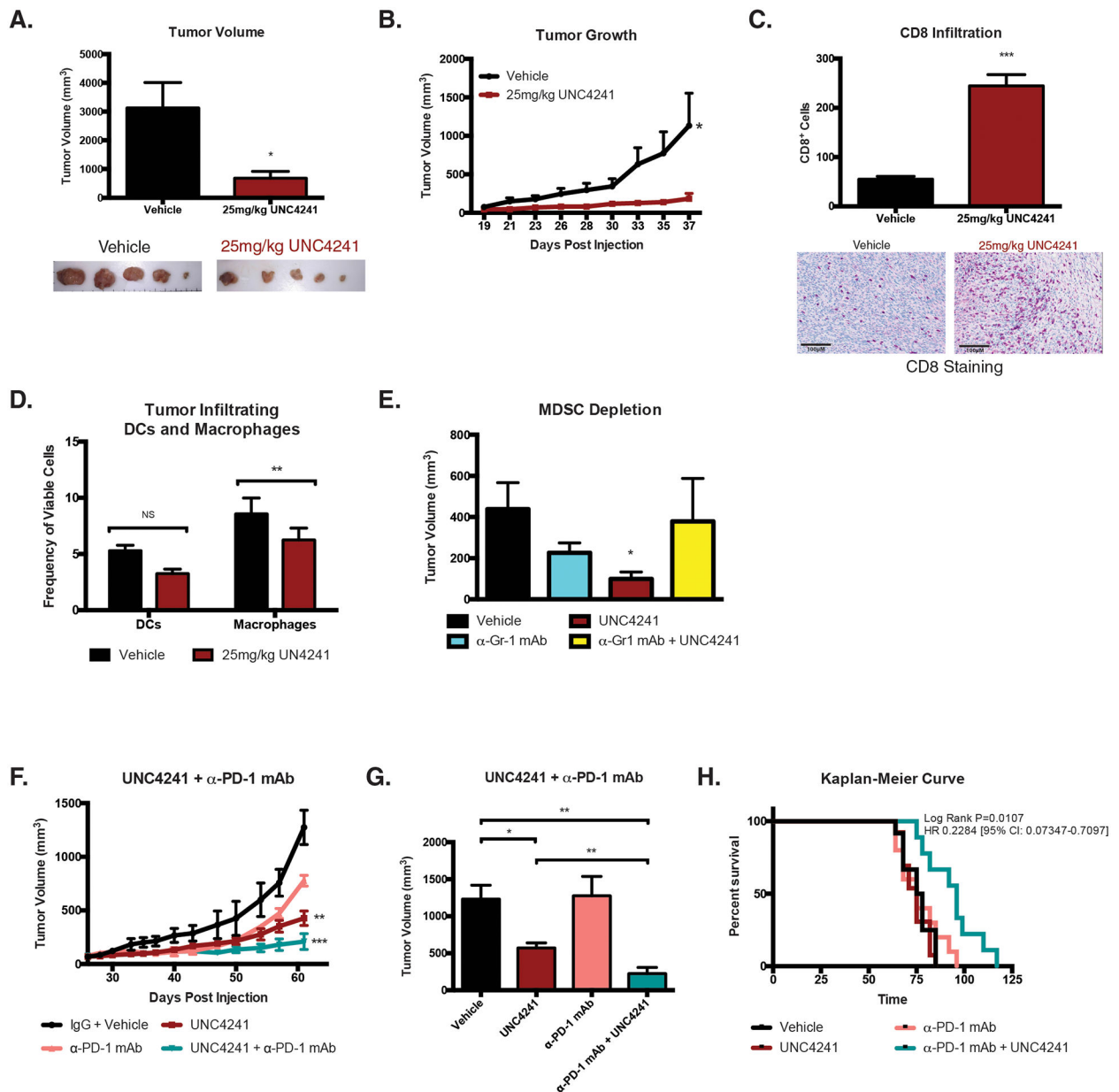**Figure 4: UNC4241 delayed tumor growth, promoted T cell infiltration and augmented anti-PD-1 therapy.**

A) Left: BRAF^{V600E}PTEN$^{-/-}$ tumors resected from mice treated with a saline vehicle or 25mg/kg UNC4241 daily. Right: Average tumor volume of tumors from mice treated with a saline vehicle or 25mg/kg UNC4241. Representative of 3 independent experiments. n=5/group *P<0.05. **B)** Tumor growth curve of tumors from mice treated with a saline vehicle or 25mg/kg UNC4241. Representative of 3 independent experiments, n=5/group. **C)** Immunohistochemistry staining of CD8 on resected BRAF^{V600E}PTEN$^{-/-}$ tumors from mice treated with a saline vehicle or 25mg/kg UNC4241. n=5 ***P<0.001. **D)** Quantification of tumor-infiltrating dendritic cells and macrophages by flow cytometry. n=9 **P<0.01. NS = not significant) **E)** Tumor volume of mice treated with saline vehicle and isotype control antibody, 200μg α-Gr-1, 25mg/kg UNC4241 or both α-Gr-1 and UNC4241. Representative

of 3 independent experiments. n=5 *P<0.05. **F-G**) Tumor volume (Day 60) and survival curve (**H**) of mice bearing BRAF^{V600E}PTEN$^{-/-}$ tumors treated with saline vehicle and isotype control antibody, 25mg/kg UNC4241 daily, 250µg α-PD-1 every 3 days or both UNC4241 (daily) and α-PD-1 (every 3 days). n=7 *P<0.05. ***P<0.001. All data are mean ± SEM. Significance calculated using the unpaired *t* test.
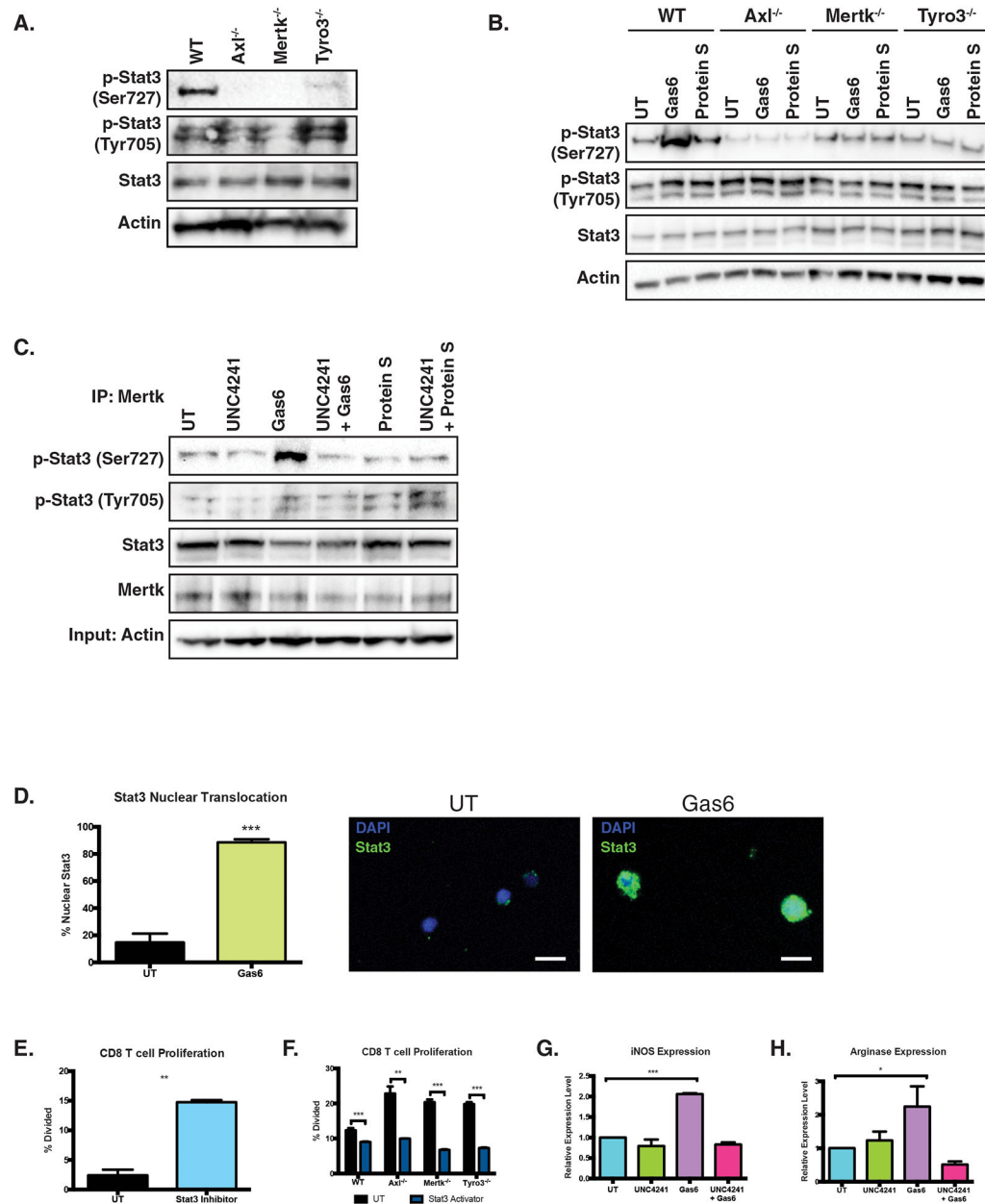
Figure 5. TAMs facilitated MDSC action through Stat3 signaling.
A) WT, *Axl*−/−, *Mertk*−/− and *Tyro3*−/− BM-MDSCs were analyzed by Western blot with the indicated antibodies. Data are representative of 3 independent experiments. **B)** BM-MDSCs were serum starved for 4 hours then treated with 200ng/ml GAS6 or 5μg/ml Protein S for 15 minutes at 37°C. Cells were lysed and analyzed by Western blot with the indicated antibodies. **C)** BM-MDSCs were serum starved for 4 hours, then pre-treated with 300nM UNC4241 for 1 hour if applicable then treated with 200ng/ml GAS6 or 5μg/ml PROTEIN S for 15 minutes at 37°C. MERTK was immunoprecipitated and samples were analyzed by Western blot using the indicated antibodies. Data are representative of 3 independent experiments. **D)** BM-MDSCs were serum starved for 2 hours then treated with 200ng/ml GAS6 for 40 minutes at 37°C. Immunofluorescent staining was performed with a STAT3

antibody and DAPI. n=11 ***P<0.001. **E)** Untreated (UT) and STAT3 inhibitor treated MDSCs' suppression of OVA-stimulated CD8$^+$ T cell proliferation measured by Cell Proliferation Dye eFluor 450 dilution. Representative of 2 independent experiments. n=3 for each experiment. **P<0.01 **F)** UT and Stat3 activator treated WT, *Axl*$^{-/-}$, *Mertk*$^{-/-}$ and *Tyro3*$^{-/-}$ MDSCs' suppression of OVA-stimulated CD8$^+$ T cell proliferation measured by Cell Proliferation Dye eFluor 450 dilution. Representative of 2 independent experiments. n=3 for each experiment **P<0.01 ***P<0.001. **G)** iNOS and Arginase (**H**) qRT-PCR analysis of MDSCs treated with 300nM UNC4241 and 200ng/ml GAS6. All data are mean ± SEM. Significance calculated using the unpaired *t* test.
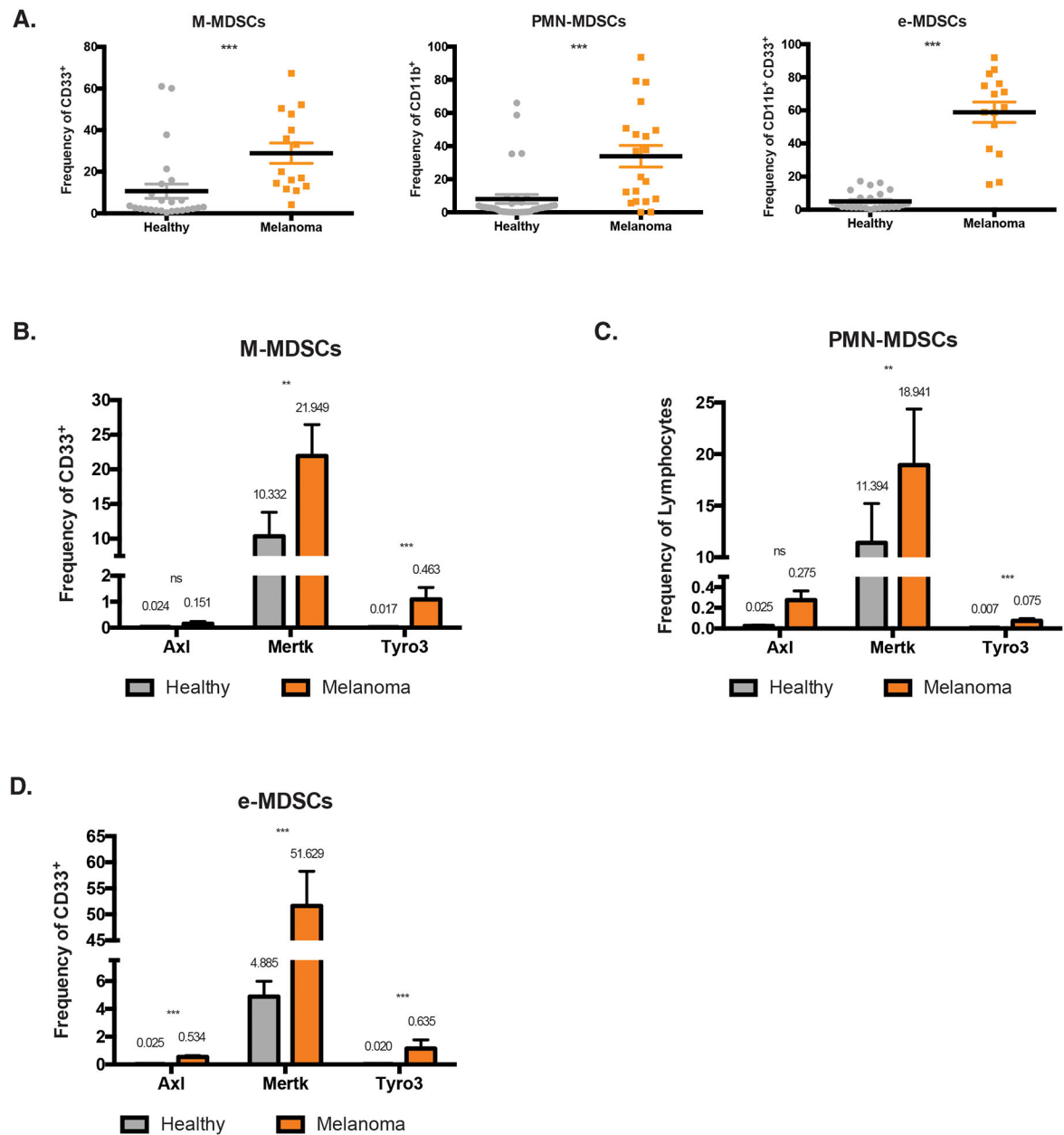
Figure 6: The frequency of TAM RTK+ MDSCs was increased in Metastatic Melanoma Patients.
A) The percentage of M-MDSCs (CD3+CD14+HLA-DR−/loCD15−), PMN-MDSCs (CD11b+CD14−CD66b+) and e-MDSCs (Lin−(CD3/14/15/19/56) HLA-DR−CD33+CD11b+) in the blood of healthy donors and metastatic melanoma patients were quantified by flow cytometry. N=25 healthy, n=15 melanoma ***P<0.001 Mann-Whitney test. The number of AXL+, MERTK+ and TYRO3+ M-MDSCs **(B)**, PMN-MDSCs **(C)**, and e-MDSCs **(D)** in the blood of healthy donors and metastatic melanoma patients were quantified by flow cytometry. n=25 healthy, n=15 melanoma ns=non-significant **P<0.01 ***P<0.001. All data are mean ± SEM. Significance calculated using the Mann-Whitney test.